Available online at www.sciencedirect.com
SCIENCE DIRECT
Polymer 46 (2005) 2889–2899
polymer
www.elsevier.com/locate/polymer

Multiple jets in electrospinning: experiment and modeling

S.A. Theron, A.L. Yarin, E. Zussman*, E. Kroll

Department of Mechanical Engineering, Technion—Israel Institute of Technology, Haifa 32000, Israel

Received 28 September 2004; received in revised form 3 December 2004; accepted 12 January 2005
Available online 5 March 2005

Abstract

The electric forces are the main factor responsible for the characteristic jet path and stretching in electrospinning. The present work describes the results of the experimental investigation and modeling of multiple jets during the electrospinning of polymer solutions. Realistic configurations of the external electric field between the electrodes were employed, as well as the linear and non-linear, Upper-Convected Maxwell, models were used to describe the viscoelastic behavior of the polymer jets. The results demonstrate how the external electric fields and mutual electric interaction of multiple charged jets influence their path and evolution during electrospinning.

Keywords: Electrospinning; Nanofibres; Multiple jets

1. Introduction

Electrospinning of polymer solutions has gain much attention in the last few years as a cheap and straightforward method to produce nanofibers [1–5]. Electrospinning differs from the traditional wet/dry fiber spinning in a number of ways, of which the most striking differences are the origin of the pulling force and the final fiber diameters. The mechanical pulling forces in the traditional industrial fiber spinning processes lead to fibers in the micrometer range and are contrasted in electrospinning by electrical pulling forces that enable the production of nanofibers [3]. Depending on the solution properties, the throughput of single-jet electrospinning systems ranges from 10 μl/min up to 10 ml/min. This low fluid throughput may limit the industrial use of electrospinning. A stable cone-jet mode followed by the onset of the characteristic bending instability, which eventually leads to great reduction in the jet diameter, necessitate the low flow rate [6].

A similar process inefficiency related to low throughput has been identified in a kindred electrospraying process (electrohydrodynamic atomization of low viscosity Newtonian fluids). However, MEMS techniques, for example, have been used to produce multi-element arrays of capillary emitters, each of which supports a single Taylor cone structure and produces a spray of charged droplets [7]. The combination of several single-jet electrohydrodynamic (EHD) atomizers becomes operationally and technically difficult. To meet high liquid throughput requirements atomizers have been designed from which multiple EHD jets originate [8] (one emitter that supports multiple Taylor cone structures). In the framework of electrospinning of polymer nanofibers, Ref. [9] provided a new approach employing a ferromagnetic liquid sublayer. In particular, a two-layer system, with the lower layer being a ferromagnetic suspension and the upper layer a polymer solution was subjected to a normal magnetic field. As a result, steady vertical spikes of magnetic suspension perturbed the interlayer interface, as well as the free surface of the uppermost polymer layer. With the addition of normal external electric field, the perturbations of the free surface became sites of jetting directed upward. This is in a sense similar to Ref. [8], since jetting occurred from a shared fluid bath and sites of jetting arranged themselves at natural intervals. Multiple emitters/nozzles have also been introduced in electrospinning as a means to increase production rate [10–14]. In addition to the increase in production rate, multiple nozzles have been used in electrospinning to make multi-component blend nanofibrous mats [12,15,16]. Furthermore, additional complexity has been added to the

* Corresponding author.
E-mail address: meeyal@tx.technion.ac.il (E. Zussman).

0032-3861/$ - see front matter © 2005 Elsevier Ltd. All rights reserved.
doi:10.1016/j.polymer.2005.01.054

nozzles in electrospinning: compound coaxial nozzles have been designed to enable the fabrication of compound core shell electrospun nanofibers [17,18].

In spite of the practical implementation of multiple jets in electrospinning in order to increase the production rate detailed physical understanding of the outcome of jet–jet interaction is still missing, as to our knowledge. The aim of the present work is the investigation of simultaneous

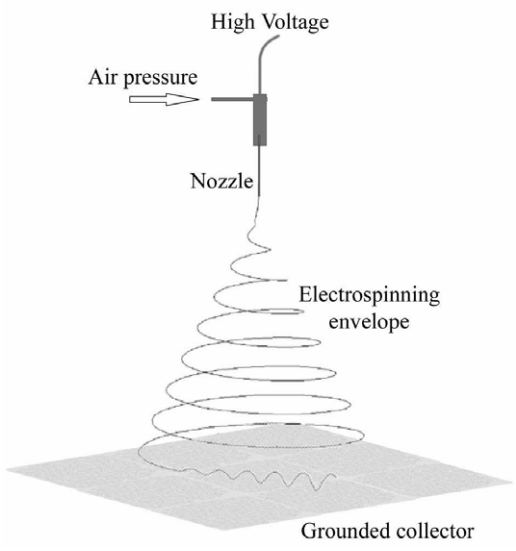

(a)

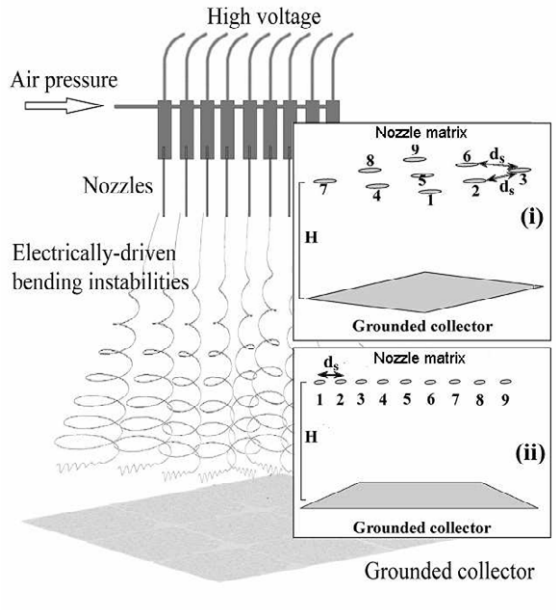

(b)

Fig. 1. Schematic drawings of single and multiple-nozzle electrospinning setups used in this work. (a) An ordinary single-jet electrospinning setup. (b) Multiple-jet electrospinning setups: (i) The nozzles in the setup were arranged in a 3×3 matrix with each nozzle attached to a syringe with polymer solution; (ii) The second multiple-jet arrangement consisted of syringes in a row (a 9×1 and a 7×1 linear array).

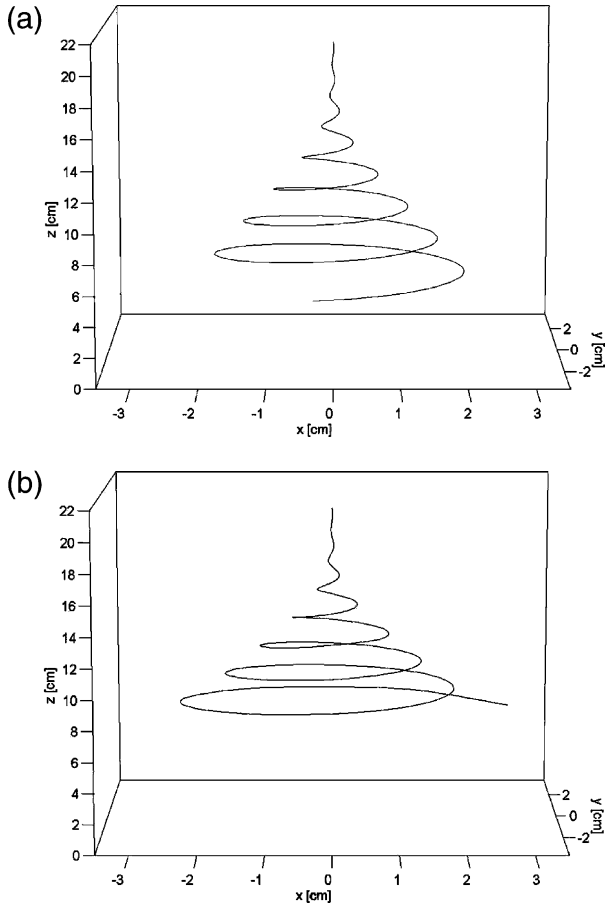

Fig. 2. The predicted jet path for single-jet electrospinning process at $t=$ 0.763 ms. The linear and Upper-Convected Maxwell models were used to describe the viscoelastic behavior in (a) and (b), respectively.

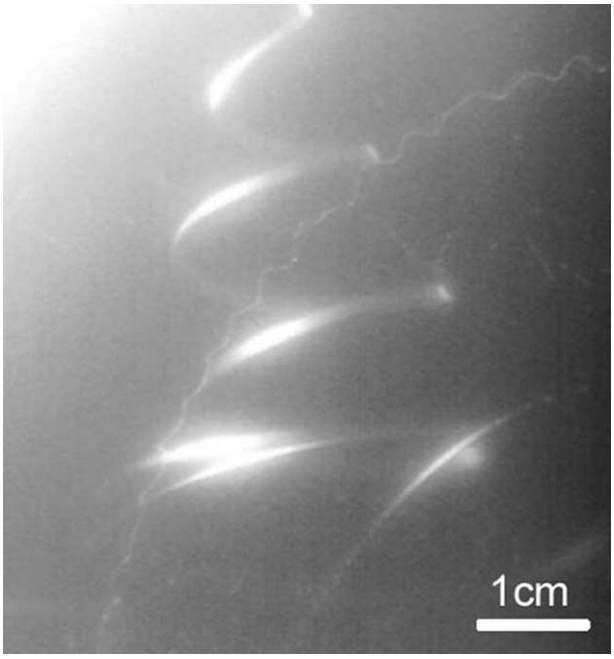

Fig. 3. Image of the electrically driven bending instability in a single-jet electrospinning process that was taken with a high speed digital camera. The photograph was taken at a shutter speed of 1 ms.

electrospinning of polymer nanofibers from multiple nozzles and the experimental and theoretical description of the jet–jet interaction. For this purpose single- and multiple-jet experimental setups were used. Section 2 details the experimental procedure and setup. The theoretical model is briefly described in Section 3. This is followed in Section 4 by presentation and discussion of the results. A summary is provided in Section 5.

2. Experimental section

2.1. Material preparation

Polyethylene oxide (PEO, Molecular weight $=6\times 10^5$ g/mol), purchased from Aldrich, was used to prepare a solution that was employed as the working fluid. The polymer powder was dissolved in water at 3% weight concentration with the aid of mechanical stirring.

2.2. Experimental setup

Several experimental setups were used during this work. The first, setup A in Fig. 1(a), was, in fact, an ordinary single-jet electrospinning setup similar to that used in previous works on electrospinning [2–6]. In the second setup (Fig. 1(b)), nine identical syringes, containing identical solutions, were arranged in two different matrix arrays as shown schematically in Fig. 1(b), (i) and (ii). At first a 3×3 matrix arrangement (setup B_i) was used and

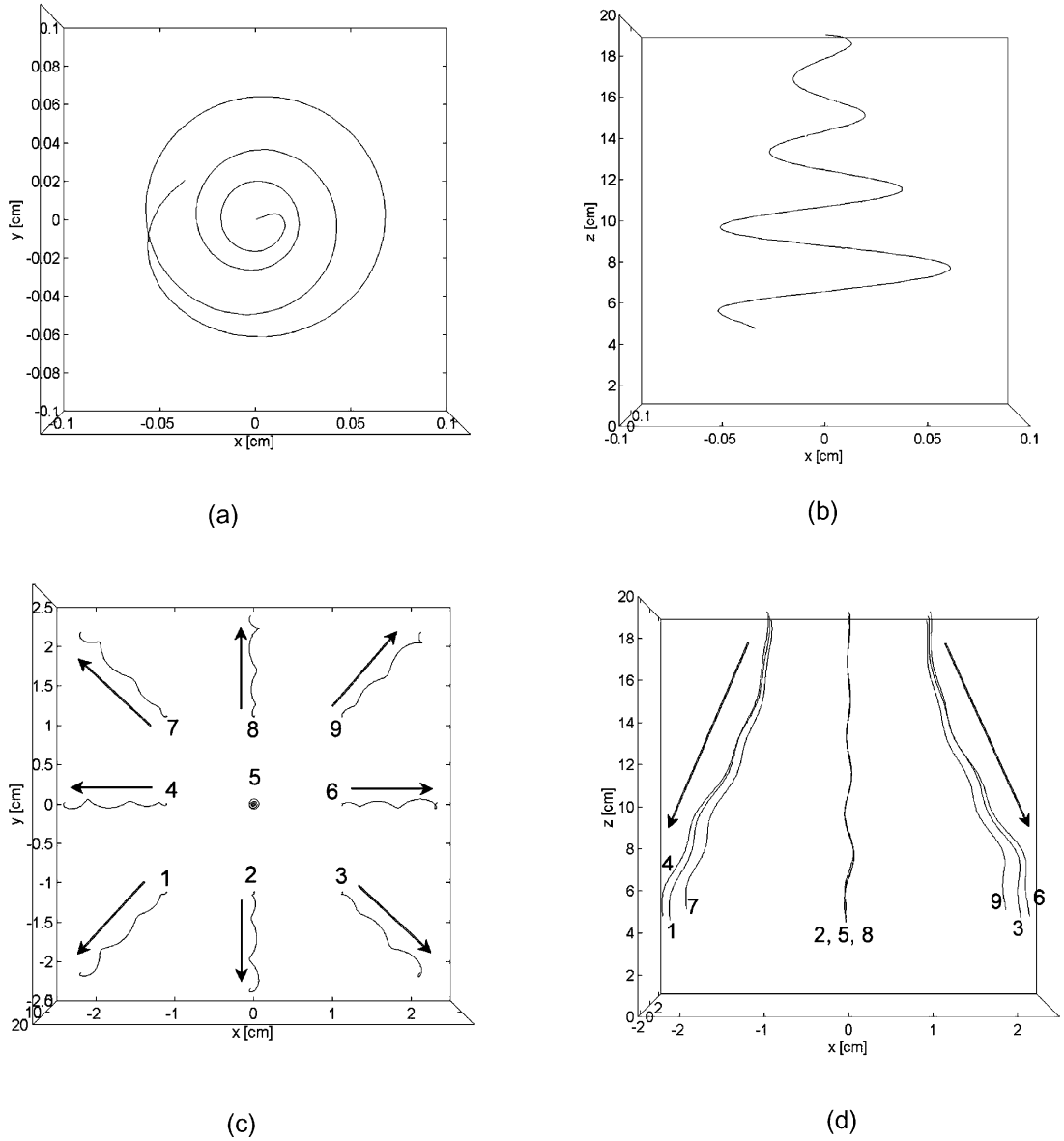

Fig. 4. The predicted paths of the nine jets in setup B_i at $t=3.4$ ms. The linear Maxwell model was used to describe the viscoelastic behavior. (a) The jet at the center of the 3×3 matrix (#5 in Fig. 1(b), setup (i)), top view; (b) Side view of jet #5; (c) Top view of all the jets of the 3×3 matrix; (d) Side view of all the jets.

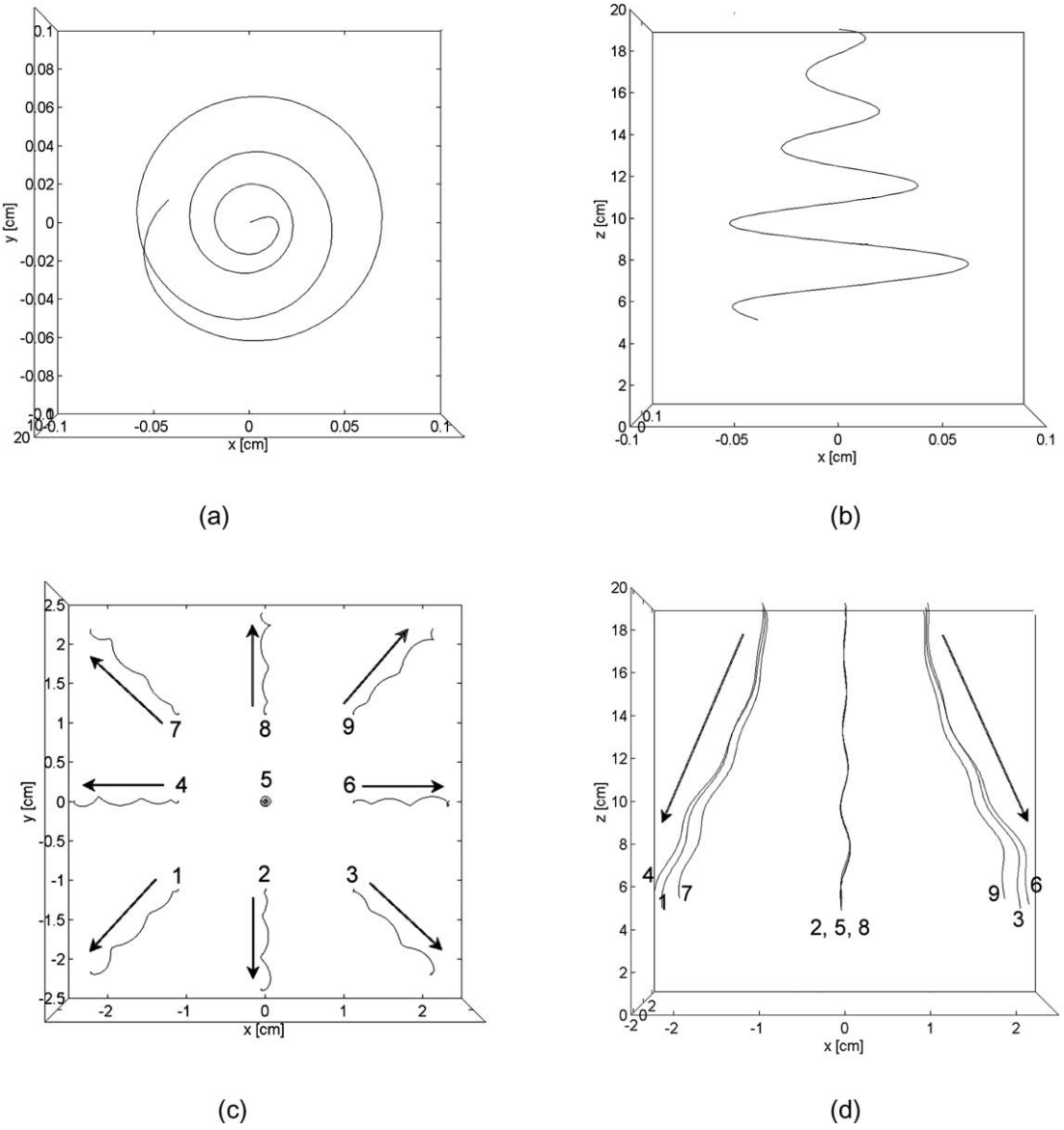

Fig. 5. Instantaneous configurations of the predicted paths of the nine jets in setup B_i at $t=3.4$ ms. The non-linear UCM model was used to describe the viscoelastic behavior. (a) The jet at the center of the 3×3 matrix (#5 in Fig. 1(b), setup (i)), top view; (b) Side view of jet #5; (c) Top view of all the jets; (d) Side view of all the jets

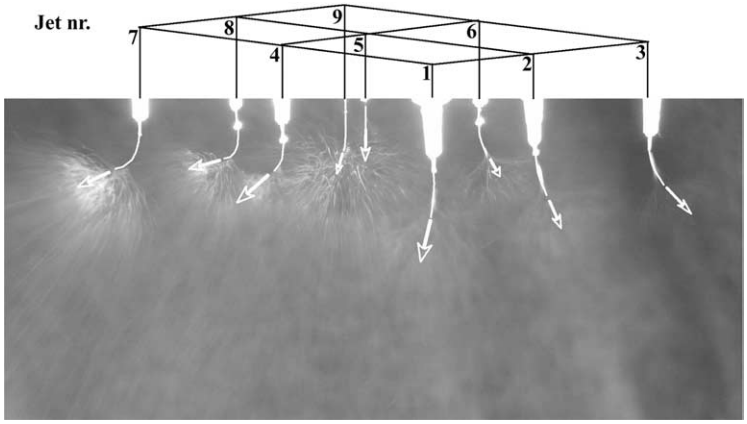

Fig. 6. A photograph of a nine-jet electrospinning process where the jets were arranged in a 3×3 matrix (setup B_i). The photograph was taken with a slow shutter speed (200 ms). Arrows indicate the three-dimensional directions of the jets' axes. The distance, d_s, between the nozzles in the image was 5 cm.

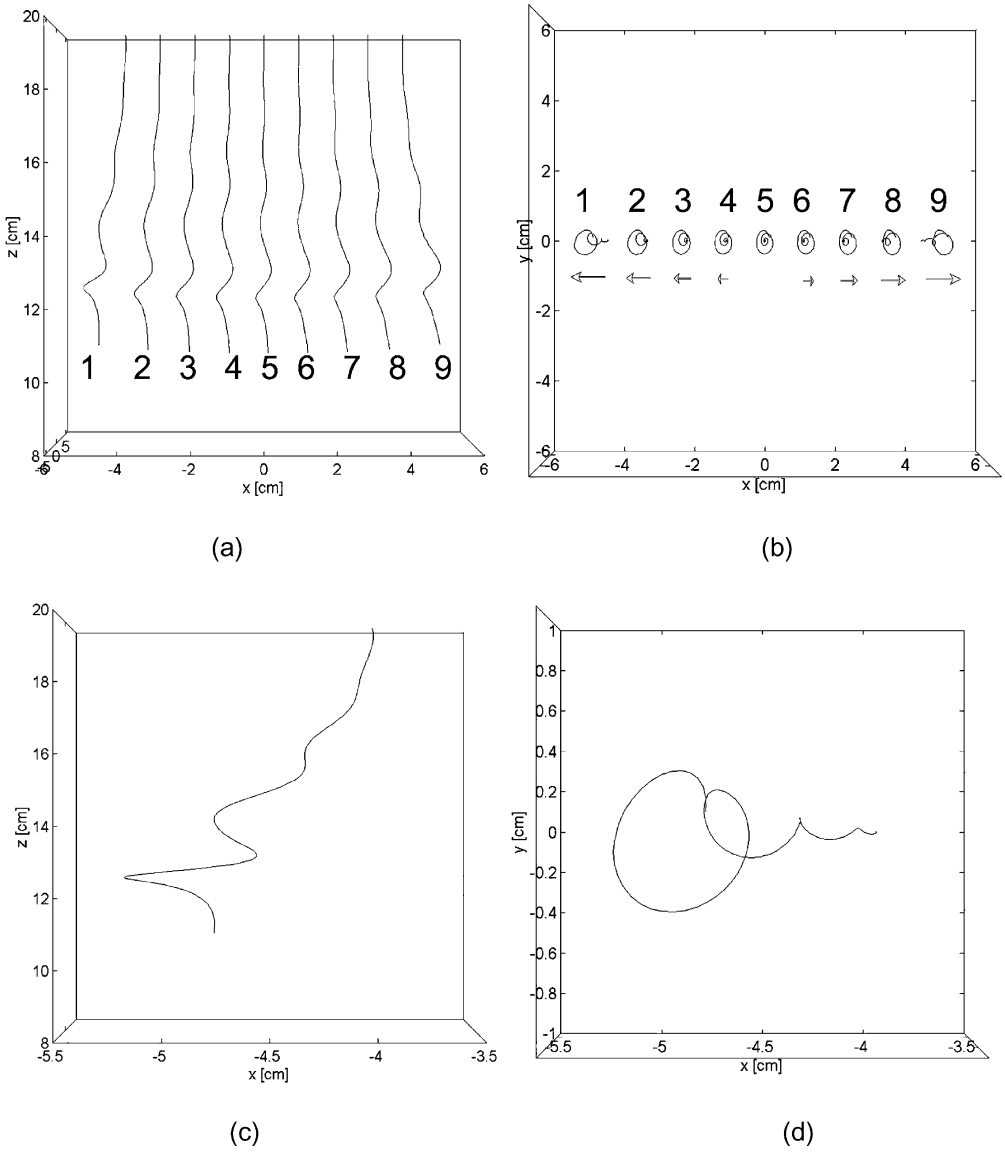

Fig. 7. The paths of nine jets in a multiple jet electrospinning process, where the jets were arranged in a row (setup B_{ii}). The linear Maxwell model was used to describe the viscoelastic behavior. These jet paths were obtained from the calculations at $t=3.4$ ms. (a) Side view of all the jets. (b) Top view corresponding to (a). (c) Side view of jet #1. (d) Top view of jet #1. (e) Side view of jet #3. (f) Top view of jet #3. (g) Side view of jet #5. (h) Top view of jet #5.

afterwards in the second setup 9×1 or 7×1 linear arrangements (setup B_{ii}) were employed. All syringes were subjected to the same applied voltage (10 kV) and to the same applied air pressure (100 mbar). A high voltage power supply (Gamma High Voltage Research, XRM30P) was used to control the applied voltage. The solution throughput was fixed by the applied voltage together with the applied air pressure inside the syringes. A hypodermic needle (inner diameter of ϕ250 μm), functioning as a nozzle, was used on every syringe. The electrospun fibers were collected on a large flat grounded collector (400 mm$\times$ 400 mm). The distance between the individual nozzles d_s was 1–5 cm. In all the setups the nozzle-to-ground distance H was 40 cm. The details of the bending instability of the electrospun jets were captured with a high-speed CCD camera (MotionScope-Redlake Imaging Corporation). The camera was equipped with a 70–180 mm, f/4.5 zoom lens. Slow shutter speed photography was used to capture the general details of the development of the jets. A single shot, digital camera (Sony DSC-F828 Cyber-shot) was used for this purpose. All solutions were stored at room temperature. All electrospinning experiments were carried out at room temperature and normal atmospheric pressure. The surrounding gas was air.

3. Modeling

A viscoelastic electrospun polymer jet is initiated at the tip of a Taylor-cone-like drop at the nozzle exit, and at the

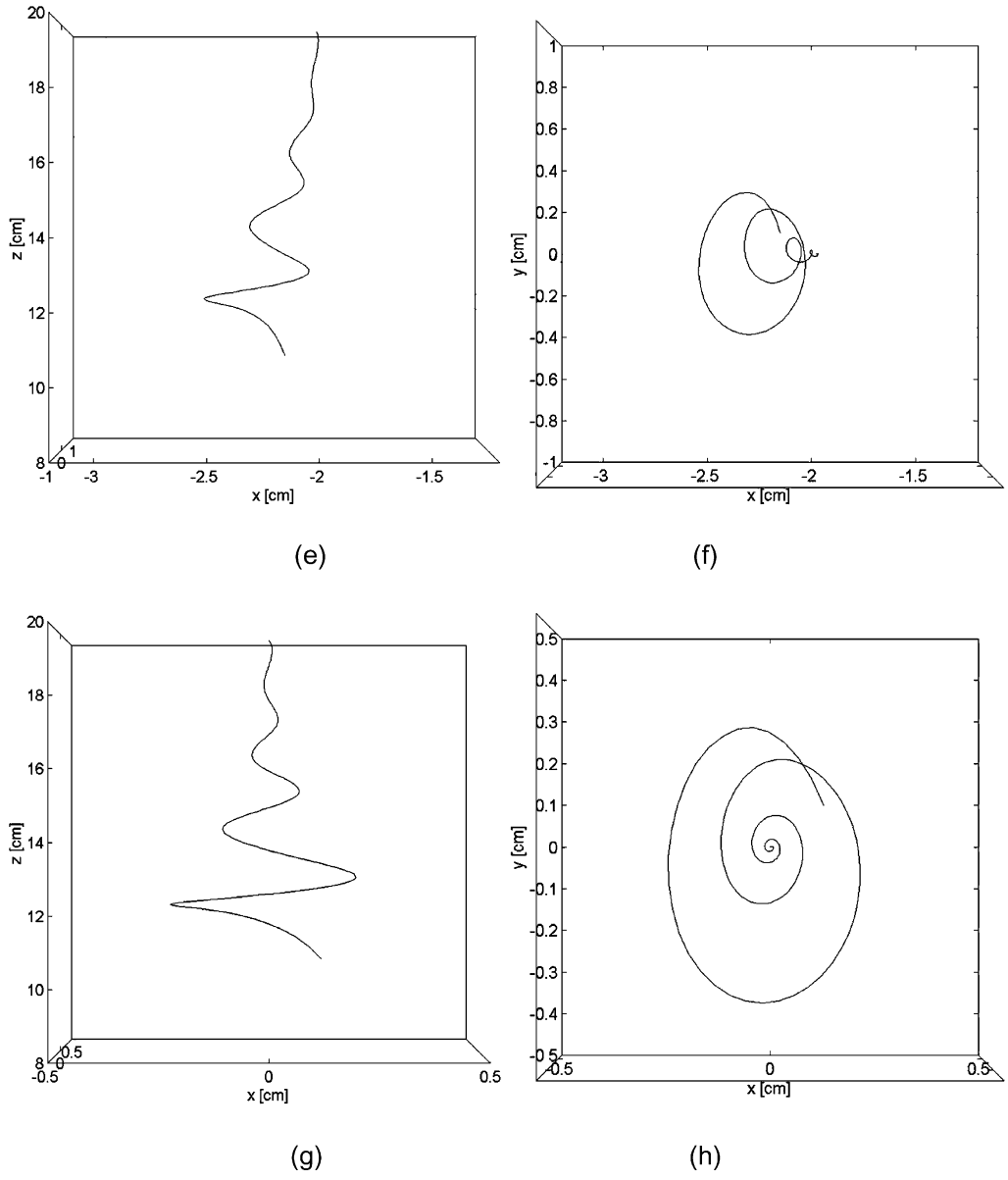

Fig. 7 (*continued*)

beginning, its path is almost straight [3,19–24]. However, at a distance of several centimeters the electrically driven bending instability sets in. As a result, jet looping begins, the jet elongates dramatically, whereas its cross-sectional radius reduces. In addition, solvent evaporates and jet solidification takes place. For a single jet these developments were modeled in the above-mentioned works. In the present note the model of Refs. [3,19] is generalized for the case of multiple bending jets with mutual Coulombic interactions. A number of additional new elements introduced in the model are briefly summarized in this section. Firstly, the uniform capacitor electric field of Refs. [3,19] was replaced in the present work with the electric field that exists between a sharp electrified nozzle and a large flat ground collector. In the simplest form this field can be represented by the field between a pointwise charge opposite to a conducting plate (or a mirror image of a charge of an opposite sign) [25]. Also, mutual Coulombic interactions between the charged jet elements are accounted for not only for a given jet (as for a single jet in Refs. [3,19]) but for all the jets in the array.

In Refs. [3,19] only the linear rheological constitutive Maxwell model was used to describe the deviatoric stress tensor. In the present work in several cases we used, in addition, the non-linear Upper-Convected Maxwell model (UCM) [26] to describe the viscoelastic behavior of polymer solutions. It was shown that UCM model provides an adequate description of the behavior of polymeric fluids in strong uniaxial elongational flows [27,28]. Electrospinning provides an example of a strong uniaxial elongational flow

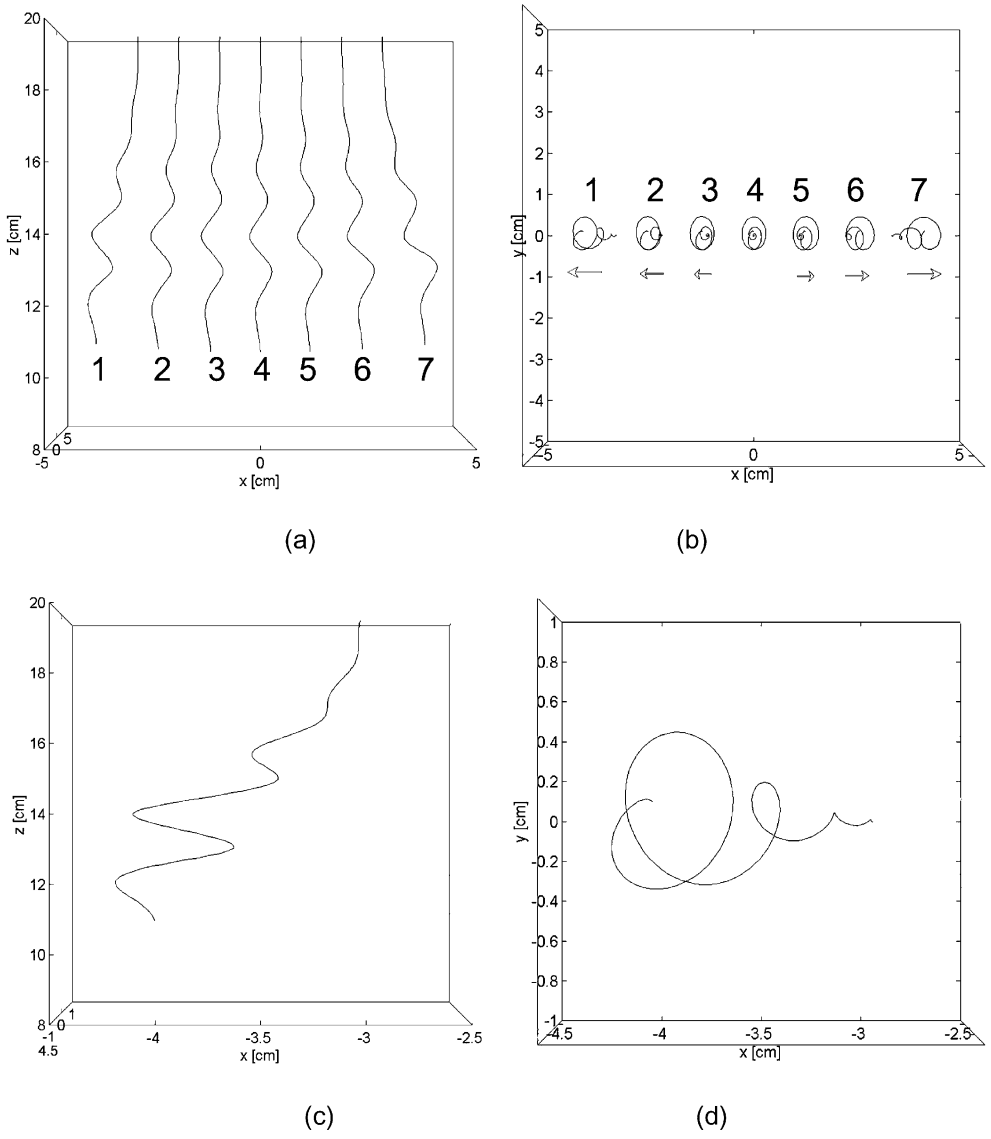

Fig. 8. The predicted paths of the seven jets in setup B_{ii} at $t=3.8$ ms. The non-linear UCM model was used to describe the viscoelastic behavior. (a) Side view of all the jets. (b) Top view of all the jets. (c) Side view of jet #1. (d) Top view of jet #1. (e) Side view of jet #3. (f) Top view of jet #3. (g) Side view of jet #4. (h) Top view of jet #4.

[3], where a quasi-one-dimensional variant of the UCM model can be employed as in the theory of viscoelastic polymer jets [28].

On the experimental level, parameter values are not fully known. Their values can only be estimated to the correct order of magnitude. Therefore our calculations were done with the order-of-magnitude-correct parameter values listed in Refs. [3,6,19,29]. In particular, in all the cases viscosity $\mu=100$ P and the relaxation time $\theta=0.1$ s. The comparison between the experiment and calculations is only on a qualitative level. Additional parameters used here include the distance between nozzles, d_s, in the case of multiple jets, and positive V_+ and negative V_- voltages assigned to the nozzle electrode and the counter electrode (ground), respectively.

4. Results and discussion

Fig. 2(a) and (b) show the calculated path of the jet in setup *A*. The external electric field was simulated by two pointwise charges opposite a large flat ground collector as described in Section 3. The linear Maxwell model and non-linear UCM model were used to calculate the viscoelasticity in Fig. 2(a) and (b), respectively. The radii of the loops of the calculated jet path shown in this figure at the moment $t=$ 0.763 ms which resulted from the electrically driven bending perturbations, are of the same order of magnitude as that found in the experiment (cf. Fig. 3). The calculated path shows only the primary bending instabilities, while in the experiment secondary bending instabilities could be observed as well. It is instructive to see that the linear

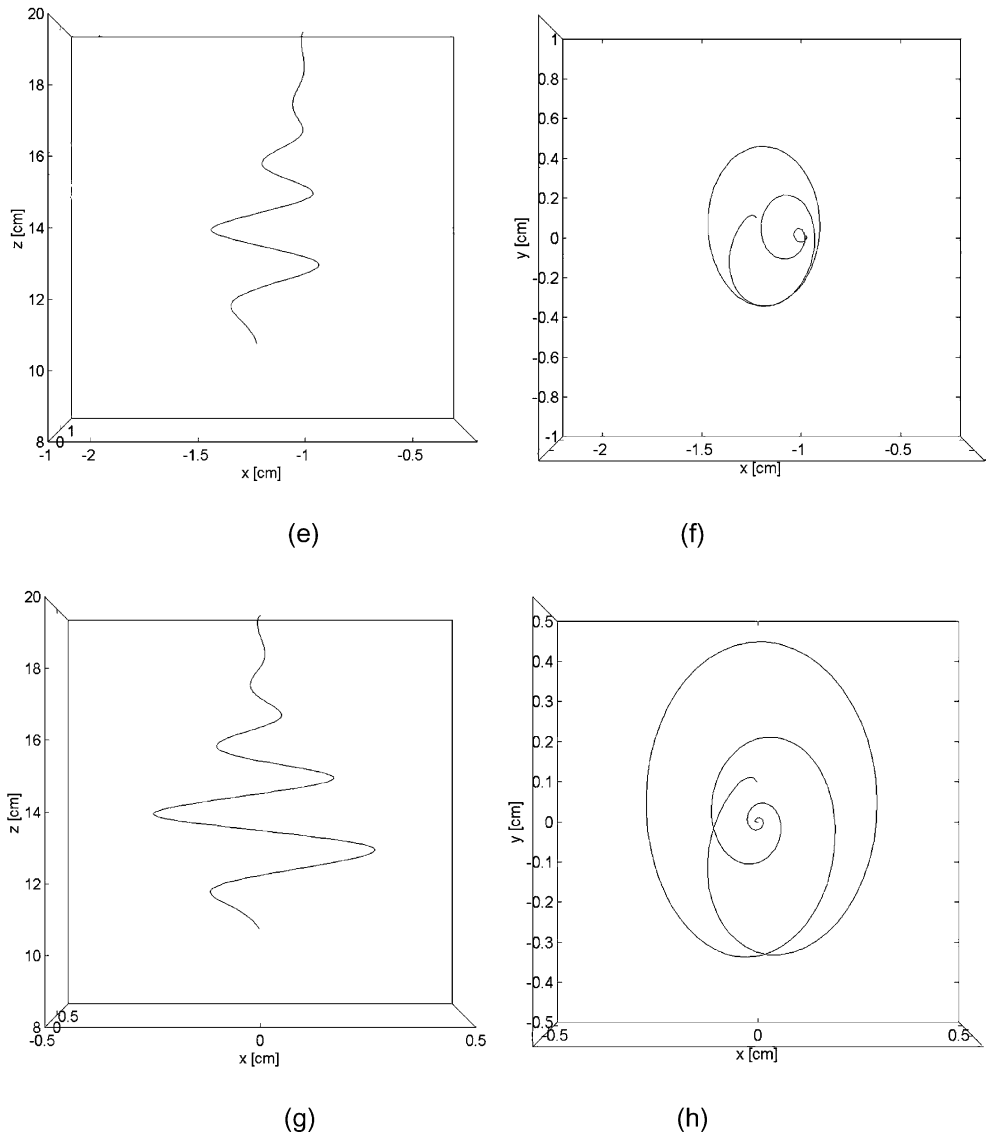

Fig. 8 (*continued*)

Maxwell model and the non-linear UCM model lead to rather close results in the flow dominated by the electric forces.

In a multiple-nozzle arrangement, not only the external applied electric field and self-induced Coulombic interactions influence the jet path, but also mutual-Coulombic interactions between different jets contribute. Fig. 4 shows the predicted paths of different jets in the multiple-jet setup B_i, where the linear Maxwell model has been utilized. For comparison the non-linear UCM model was implemented for the calculations in Fig. 5. Once more, it is seen that the behavior of the jets predicted by two different rheological models is quite similar. Namely, the central jet #5 in both cases (cf. Figs. 4(a), (b) and 5(a), (b)) develops like one would expect of a jet in a single-jet process. Figs. 4(c) and 5(c) show a top view of all the jets. The arrows in these figures indicate in which direction the jets paths are bent. A side view of the paths in Figs. 4(c) and 5(c) is given in Figs. 4(d) and 5(d). The central jet (#5) develops downward being restricted by the jets on its side (#1, 2, 3, 4, 6, 7, 8 and 9), while those on the sides are pushed outward away from the center. It is thus clear that the jets on the sides of the matrix also undergo bending and looping but in addition their paths are pushed away from the other jets in a direction radially outward from the central jet #5, as indicated by the arrows. The behavior of the different jets, predicted by the model in Figs. 4 and 5, is clearly visible in the experiment with setup B_i (cf. Fig. 6). Mutual repulsion of electrospun jets is even clearer in the linear-array (row) arrangement that is discussed next.

The calculated paths for the jets in setup B_{ii} are shown in Fig. 7 (a 9×1 nozzle linear arrangement) and in Fig. 8 (a 7×1 nozzle linear arrangement). In Fig. 7 the viscoelastic behavior was modeled with a linear UCM model and in

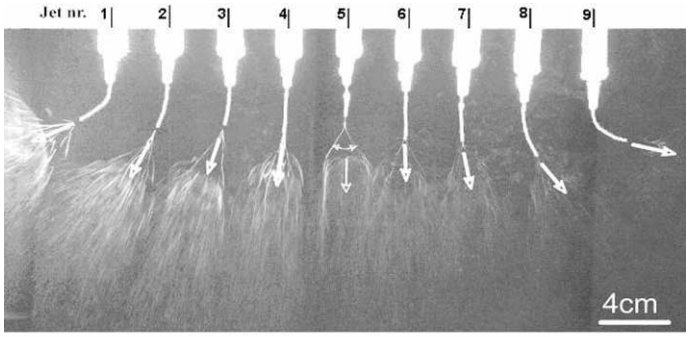

(a)

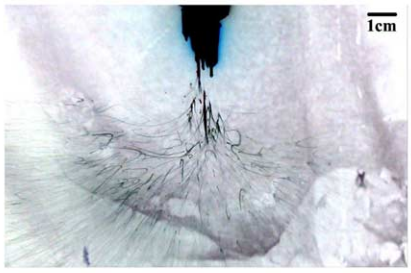

(b)

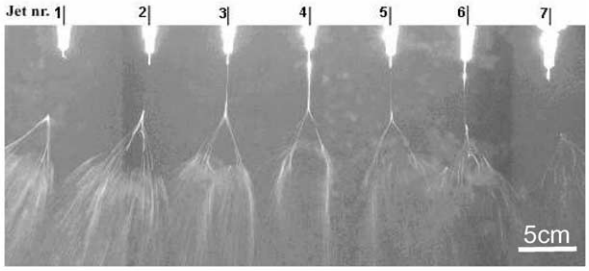

(c)

Fig. 9. Photographs taken at long exposure times (200 ms) of a nine-jet electrospinning process using setup B_{ii}. The distance between the individual syringes is 4 cm. (a) Front view of jets #1 to 9 with arrows to indicate the direction of the main axes of the electrospinning envelopes. (b) A side view of all the jets. Jet #1 is the foremost jet in the image. (c) Front view of jets #1 to 7 in setup B_{ii} with seven nozzles in a row.

Fig. 8 the non-linear UCM model was employed. The inter-nozzle distance in the calculations was 1 cm. Figs. 7 and 8 show that predictions indicate that every jet in the multi-jet configurations undergoes the characteristic bending instability. Also the calculated paths in Figs. 7(a), (b) and 8(a), (b) show that the closer the jet is to the edge of the linear array of setup B_{ii}, the stronger it bends outward in the direction indicated by the arrows in these figures. This can also be seen when one compares the path of jet #1 (cf. Figs. 7(c), (d) and 8(c), (d)) and of jet #3 (cf. Figs. 7(e), (f) and 8(e), (f)). The jet in the center of the linear arrays (jet #5 in Fig. 7(a), (b), (g) and (h) and jet #4 in Fig. 8(a), (b), (g) and (h)) develops downward. Furthermore the calculations predict that the envelope cones of the inner jets are squeezed along the line on which the jets are located. This phenomenon is clearly visible in Figs. 7(a), (h) and 8(a), (h), which reveal that the diameter of the inner envelope cones is larger in the direction perpendicular to the line on which the jets are located than in the direction parallel to the latter. Experimental observations of the jets paths for setup B_{ii} corresponding to the modeling results in Figs. 7 and 8 are shown in Fig. 9. From Fig. 9(a) and (c) it is clear that, as predicted, the closer the jet is to the edge of the linear array, the stronger it bends outward. Furthermore, the semi-vertical angle of the electrospinning envelope cones, of the two jets on the edges, is slightly larger than for the inner jets (#2–8 in Fig. 9(a)). The values of the latter angles, given in Table 1, were obtained by measuring the semi-vertical angle between the two bright lines bifurcating for a specific jet envelope in Fig. 9(a). In Fig. 9(a) the measured angle for jet #5 is indicated by a double headed arrow. The semi-vertical angle of the electrospinning envelope for the inner jets lies between 25° and 30°. When rotating Fig. 9(a) by 90° (side view), the semi-vertical angle of the envelope cone in the direction perpendicular to the line on which the nozzles are located, is revealed. The latter angle, estimated from

Table 1
Semi-vertical angles of the electrospinning envelope cones measured for the jets in Fig. 9(a)

Jet nr.	1	2	3	4	5	6	7	8	9
Angle (Fig. 9(a))	40°	28.5°	25.5°	30°	29°	27.5°	29°	29°	33.5°

Fig. 9(b), is between 50° and 75°. This confirms that the inner envelope cones are, in fact, squeezed along the line on which the nozzles are located. Although the electrospinning envelopes are squeezed, the electrically driven bending instability of all the jets is similar to the one familiar for single jets.

5. Summary

The behavior of jets in multiple-jet electrospinning processes, which are necessitated by mass production requirements of electrospun fibrous mats, was investigated. It has been demonstrated experimentally and with the help of numerical simulations that the mutual Coulombic interactions influence the paths of individual electrified jets in electrospinning. The simulations were done in the framework of the model of Refs. [3,19] generalized for the case of multiple jets interacting via Coulombic forces. Also, in addition to the linear Maxwell model employed in Refs. [3,19], the non-linear Upper Convected Maxwell model was used to describe viscoelastic rheological behavior of polymer solutions in a number of simulations in this work. The results of the modeling suggest that both the non-linear UCM model and the linear Maxwell model implemented in Refs. [3,19], provide a reasonable and quite close description of the viscoelastic behavior of jets in electrospinning. Several more realistic configurations of the applied electric field were employed in the present work as well. It was found both experimentally and in the simulations, that mutually interacting jets in an arrangement still undergo bending instabilities characteristic of electrospinning. In addition, it was found that the jets are pushed away from their neighbors by the Coulombic forces applied by the latter. In the case of a double-jet electrospinning process, the repulsion of the jets results in the collection of a non-uniform non-woven mat. The effect, however, is reduced by the introduction of more jets. In large two-dimensional matrices of jets, the inner jets develop in the same way as jets in single-jet electrospinning processes, which leads to uniformity of the produced non-woven mat.

A decrease in the inter-nozzle distances d_s leads to greater repulsion between the jets. On the other hand, in the case of a large number of jets, closeness of the jets results in an increased deposition rate over a smaller area. However, with the decrease in the inter-nozzle distance, the onset of the electrically driven bending instability, which is the main factor responsible for the reduction of the fiber diameter to the nanometer scale, is delayed. In order to compensate for this delay, the nozzle-to-ground distance should be increased, which will result in an increase in the collection area. Such an interaction between the parameters in electrospinning has already been demonstrated in [6], as knowledge thereof is important for the development of sophisticated production methods. Other particular phenomenon, which was predicted as well as observed, in the case of several jets electrospun in a row, include the squeezing of the envelope cones of the inner jets along the line on which the nozzles were located.

Reasonable stability of the process and uniformity of the as-spun nanofiber mats can be achieved with an inter-nozzle distance of about 1 cm with nine nozzles on a square of about 4 cm^2. This results in the jet distribution density of 2.25 jets/cm^2, and in the production rate in the range of 22.5 l/(cm^2 min) to 22.5 ml/(cm^2 min) per 1 cm^2 of the spinneret plate.

Acknowledgements

The authors wish to acknowledge the support of this research by the Israel Science Foundation, the Israel Academy of Sciences, Grants No. 287/00-1 and 26/03.

References

[1] Baumgarten PK. Electrostatic spinning of acrylic microfibers. J Colloid Interface Sci 1971;36:71–9.
[2] Doshi J, Reneker DH. Electrospinning process and applications of electrospun fibers. J Electrostat 1995;35:151–60.
[3] Reneker DH, Yarin AL, Fong H, Koombhongse S. Bending instability of electrical charged liquid jets of polymer solutions in electrospinning. J Appl Phys 2000;87:4531–47.
[4] Bognitzki M, Czando W, Frese T, Schaper A, Hellwig M, Steinhart M, Greiner A, Wendorff JH. Nanostructured fibers via electrospinning. Adv Mater 2001;13:70–2.
[5] Zussman E, Theron A, Yarin AL. Formation of nanofiber crossbars in electrospinning. Appl Phys Lett 2003;82:973–5.
[6] Theron A, Zussman E, Yarin AL. Experimental investigation of the governing parameters in the electrospinning of polymer solutions. Polymer 2004;45:2017–30.
[7] Stark J, Stevens B, Kent B, Sandford M, Alexander M. Microfabrication and operation nano emitters suitable for a colloid thruster array. European space components information exchange system's 4th round table on micro/nano technologies for space, Noordwijk, The Netherlands, May 2003. (https://esBies.org/public/mnt4/S9.1Stark.pdf).
[8] Almekinders JC, Jones C. Multiple jet electrohydrodynamic spraying and applications. J Aerosol Sci 1999;30:969–71.
[9] Yarin AL, Zussman E. Upward needleless electrospinning of multiple nanofibers. Polymer 2004;45:2977–80.
[10] Formhals A. Process and apparatus for preparing artificial threads. US Patent 1934; 1975504.

[11] Simons HL. Process and apparatus for producing patterned non-woven fabrics. US Patent 1966; 3280229.
[12] Smith DJ, Reneker DH, McManus AT, Schreuder-Gibson AL, Mello C, Sennett MS. Electrospun fibers and an apparatus therefore. US Patent 2004; 6753454.
[13] Chu B, Hsiao BS, Fang D. Apparatus and methods for electrospinning polymeric fibers and membranes. US Patent. 2004; 6713011.
[14] Chung HY, Hall JRB, Gogins MA, Crofoot DG, Weik TM. Polymer, polymer microfiber, polymer nanofiber and applications including filter structures. US Patent 2004; 6743273.
[15] Gupta P, Wilkes GL. Some investigations on the fiber formation by utilizing a side-by-side bicomponent electrospinning approach. Polymer 2003;44:6353–9.
[16] Ding B, Kimura E, Sato T, Fujita S, Shiratori S. Fabrication of blend biodegradable nanofibrous nonwoven mats via multi-jet electrospinning. Polymer 2004;45:1895–902.
[17] Sun Z, Zussman E, Yarin AL, Wendorff JH, Greiner A. Compound core-shell polymer nanofibers by co-electrospinning. Adv Mater 2003;15:1929–32.
[18] Li D, Xia Y. Direct fabrication of composite and ceramic hollow nanofibers by electrospinning. Nano Lett. 2004;4:933–8.
[19] Yarin AL, Koombhongse S, Reneker DH. Bending instability in electrospinning of nanofibers. J Appl Phys 2001;89:3018–26.
[20] Yarin AL, Koombhongse S, Reneker DH. Taylor cone and jetting from liquid droplets in electrospinning of nanofibers. J Appl Phys 2001;90:4836–46.
[21] Hohman MM, Shin M, Rutledge G, Brenner MP. Electrospinning and electrically forced jets I: stability theory. Phys Fluids 2001;13: 2201–20.
[22] Hohman MM, Shin M, Rutledge G, Brenner MP. Electrospinning and electrically forced jets II: applications. Phys Fluids 2001;13:2221–36.
[23] Feng JJ. The stretching of an electrified non-Newtonian jet: a model for electrospinning. Phys Fluids 2002;14:3912–26.
[24] Yarin AL. Electrospinning of nanofibers from polymer solutions and melts. Lecture notes no. 5. Warsaw: Amas Publications; 2003.
[25] Smythe WR. Static and dynamic electricity. 3rd ed. New York: McGraw-Hill; 1968.
[26] Bird RB, Amstrong RC, Hassager O. 2nd ed Dynamics of polymeric liquids. vol. 1. New York: Wiley-Interscience; 1987.
[27] Yarin AL. Strong flows of polymeric liquids: 1. Rheological behavior. J Non-Newtonian Fluid Mech 1990;37:113–38.
[28] Yarin AL. Free liquid jets and films: hydrodynamics and rheology. New York: Longman and Wiley; 1993.
[29] Reznik SN, Yarin AL, Theron A, Zussman E. Transient and steady shapes of droplets attached to a surface in strong electric field. J Fluid Mech 2004;516:349–77.